

INVITED REVIEWS

The spiral structure of the Milky Way

Ye Xu¹, Li-Gang Hou^{2,3} and Yuan-Wei Wu⁴

¹ Purple Mountain Observatory, Chinese Academy of Sciences, Nanjing 210008, China; xuye@pmo.ac.cn

² CAS Key Laboratory of FAST, National Astronomical Observatories, Chinese Academy of Sciences, Beijing 100101, China

³ National Astronomical Observatories, Chinese Academy of Sciences, Beijing 100101, China

⁴ National Time Service Center, Key Laboratory of Precise Positioning and Timing Technology, Chinese Academy of Sciences, Xi'an 710600, China

Received 2018 September 3; accepted 2018 October 9

Abstract The morphology and kinematics of the spiral structure of the Milky Way are long-standing problems in astrophysics. In this review we firstly summarize various methods with different tracers used to solve this puzzle. The astrometry of Galactic sources is gradually alleviating this difficult situation caused mainly by large distance uncertainties, as we can currently obtain accurate parallaxes (a few μas) and proper motions ($\approx 1 \text{ km s}^{-1}$) by using Very Long Baseline Interferometry (VLBI). On the other hand, the *Gaia* mission is providing the largest, uniform sample of parallaxes for O-type stars in the entire Milky Way. Based upon the VLBI maser and *Gaia* O-star parallax measurements, nearby spiral structures of the Perseus, Local, Sagittarius and Scutum Arms are determined in unprecedented detail. Meanwhile, we estimate fundamental Galactic parameters of the distance to the Galactic center, R_0 , to be $8.35 \pm 0.18 \text{ kpc}$, and circular rotation speed at the Sun, Θ_0 , to be $240 \pm 10 \text{ km s}^{-1}$. We found kinematic differences between O stars and interstellar masers: the O stars, on average, rotate faster, $> 8 \text{ km s}^{-1}$ than maser-traced high-mass star forming regions.

Key words: Galaxy: structure — Galaxy: kinematics and dynamics — masers — techniques: high angular resolution — astrometry — stars: formation

1 INTRODUCTION

The Milky Way was proposed to be a spiral galaxy soon after the discovery of spiral structures in M51 (Alexander 1852) more than one and a half centuries ago. However, the Galactic spiral structure is extremely difficult to depict because the Solar System is deeply embedded in the Galactic disk. Galactic rotation was revealed by Oort in the 1920s (Oort 1927), and a major breakthrough towards understanding the Galactic spiral structure happened in the 1950s – Morgan and his colleagues found three spiral arm segments in the solar neighborhood using photometry (Morgan et al. 1952, 1953). Unfortunately, in the optical band, interstellar dust along the line of sight prevents us from determining the large scale Galactic spiral pattern beyond a few kpc from the Sun. Alternatively, obser-

ventions in radio bands, e.g., HI and CO molecular lines, which are free from being affected by dust extinction, offer new opportunities to investigate the Galactic spiral structure. However, the kinematic distances derived from rotation curves have large errors, imposing large uncertainties on the identification of spiral arms.

More than 100 models have been proposed to explain the Galactic spiral pattern, but most of them employed kinematic distances. The uncertainties mainly come from three causes: (1) difficulties in determining an accurate rotation curve, (2) kinematic distance ambiguities¹, and (3) deviations from non-circular rotation (e.g., streaming

¹ For a source in the inner Galaxy whose distance to the GC is less than the distance between the Sun and the GC, R_0 , there exist two possible distances corresponding to one observed velocity with respect to the Local Standard of Rest, V_{LSR} .

motions). These factors yield uncertainties comparable to the gaps between arms. For instance, for the molecular cloud G9.62+0.20, its far and near kinematic distances are approximately 15 and 0.5 kpc, respectively, but its true distance is about 5.7 kpc (Sanna et al. 2009). Therefore, it is hard to determine precise locations of molecular clouds and to construct the morphology of Galactic spiral arms. Up to now, there is no general consensus on the number of arms, their locations, orientations or properties.

Recently, substantial progress in our knowledge of the spatial and kinematic properties of Galactic structure has been achieved. For example, Xu et al. (2006) and Honma et al. (2007) demonstrated that Very Long Baseline Interferometry (VLBI) can obtain trigonometric parallax accuracies down to a few μas , allowing precise distance measurements towards masers throughout the Galaxy, which was recognized as a milestone in this field (Binney 2006; Caswell 2012). Large portions of spiral arms have now been accurately defined in the northern hemisphere (e.g., Reid et al. 2014; Xu et al. 2016), and in addition, the distance to the Galactic Center (GC) and the Galactic rotation speed at the Sun have been well determined (Honma et al. 2012; Reid et al. 2014).

On the other hand, the *Gaia* satellite, launched in 2013, is collecting the most precise astrometric measurements for billions of stars in the Milky Way, and the *Gaia* mission recently released its second data set (Data Release 2, DR2), containing more than one billion stars that have parallaxes and proper motions measured by *Gaia* Collaboration et al. (2016, 2018). The parallax uncertainty in *Gaia* DR2 is typically 30 μas . With a large number of parallax-measured OB stars, the spiral pattern within 3 kpc from the Sun could be revealed clearly for the first time (Xu et al. 2018).

In this review, we present the results from multiple tracers proposed over the past half century, including ionized hydrogen, neutral atomic hydrogen, molecular gas, young open clusters and particularly the results from maser trigonometric parallax. Additionally, we describe our latest research results about the stretch of spiral arms and their space motions, and Galactic fundamental parameters based on maser and O-type star parallax and proper motion measurements.

2 AN OVERVIEW OF VARIOUS TRACERS

There are roughly two kinds of spiral arms, one of which is associated with young objects, such as OB stars and

young stellar associations. Such spiral arms are birthplaces of stars, and consequently, giant molecular clouds (GMCs), young open clusters and photodissociation regions are the best tracers of this type of arm. However, the other kind is mainly traced by more evolved stars, which have moved out of their birthplaces and form another kind of spiral arm. In addition, atomic gas is characterized by 21 cm HI emissions which, due to its wide range, traces spiral arms on a larger scale. In external galaxies, the spiral arms traced by HI are similar to CO molecular gas in general, but with detailed differences (Westpfahl 1998). However, most researchers prefer combining all the tracers to just outline a single spiral arm pattern.

2.1 OB Stars and Their HII Regions

The first spiral structure was found in M51, a nearby galaxy, based on observations of high-mass stars and bright HII regions (Rosse 1850). In the Milky Way, OB stars and young stellar associations are also primary tracers of spiral arms, especially their associated HII regions, which are bright in radio wavelengths and almost immune to interstellar dust extinction, and they can be widely detected throughout the entire Galactic plane (e.g., as far as more than 20 kpc away from the observer, Anderson et al. 2012).

The global spiral arms depicted by massive young stellar objects (MYSOs) (e.g., Georgelin & Georgelin 1976; Russeil 2003; Hou & Han 2014) provide a starting point for some well-known models of the Milky Way, e.g., the electron-density models (Cordes & Lazio 2002; Yao et al. 2017), the model of dust distribution (Drimmel & Spergel 2001) and the large-scale magnetic field structure model throughout the Galactic disk (e.g., Han et al. 2018). The distances of spiral tracers are key parameters to map the Galaxy's spiral arms. The most reliable and direct method of determining the distances of MYSOs is to measure the trigonometric parallax of their associated methanol/water masers (e.g., Xu et al. 2006; Hachisuka et al. 2006). The spectrophotometry of high-mass stars in HII regions, which is based on interstellar extinction laws, is also a good method and has determined stellar distances for about 400 HII regions (e.g., Russeil 2003; Foster & Brunt 2015). For large samples (more than 1200, e.g., see Hou & Han 2014) of Galactic HII regions and masers in high-mass star forming regions (HMSFRs), only kinematic distances were esti-

mated from their V_{LSR} by using a mean Galaxy rotation curve.

We briefly review the time line of Galactic spiral arm studies. Using O and early B stars, Morgan and his collaborators first outlined parts of nearby spiral arms, three short spiral arm segments, with spectroscopic parallaxes (e.g., Morgan et al. 1952, 1953). Based on the distributions of OB stars and optical/radio HII regions, Bok et al. (1970) mapped the Carina spiral feature in Galactic longitude from 285° to 295° . Using a sample of about 160 HII regions with spectrophotometric or kinematic distances, Crampton & Georgelin (1975) identified four spiral arm segments. Georgelin & Georgelin (1976) determined the positions of 100 clusters of HII regions by spectrophotometric or kinematic distances of 360 exciting stars. These HII regions are proposed to reside in part of four spiral arms, i.e., the Perseus Arm, the Sagittarius-Carina Arm, the Scutum-Crux-Centaurus Arm and the Norma Arm. Fich & Blitz (1984) made a similar map but using more than 100 HII regions with spectrophotometric distances (their fig. 2). Avedisova (1985) obtained four clear spiral arm segments within about 6 kpc of the Sun (their fig. 3) with spectrophotometric distances known for 255 HII regions, but the data were not released. Russeil (2003) updated the stellar distances for 204 star forming complexes. Foster & Brunt (2015) determined the spectrophotometric distances to 103 HII regions in the second and third Galactic quadrants. The distance accuracy of the spectrophotometric method is not as good as that of trigonometric parallax, but the spectrophotometric method still provides relatively accurate distances with uncertainties of about 20% (e.g., Russeil 2003), and has been used to measure the mean Galaxy rotation curves (e.g., Brand & Blitz 1993; Russeil 2003). Due to absorption by dust, optical methods are limited to nearby spiral structures and are ineffective at distances greater than a few kpc, as shown in Figure 1 left. About 400 HII regions in total, within about 6 kpc of the Sun, trace part of the Perseus Arm, the Local Arm, the Sagittarius-Carina Arm and the Scutum-Crux-Centaurus Arm.

The paradigmatic map of Galaxy spiral arms was given by Georgelin & Georgelin (1976) who first proposed that the Milky Way probably has four major spiral arms. It is noted that in their model, the Local Arm was a spur or a branch, not a major arm. Downes et al. (1980) and Caswell & Haynes (1987) extended the four-arm model by observing 171 and 316 HII regions in the northern and southern sky, respectively. To update the

global maps of spiral arms, Russeil (2003) cataloged 481 star forming complexes and determined their spectrophotometric or kinematic distances. The fitted model confirmed the four-segment model of Georgelin & Georgelin (1976). Similar work was done by Paladini et al. (2004) with 550 HII regions, by Hou et al. (2009) with 814 HII regions and also by Urquhart et al. (2014) with about 1750 embedded young massive stars. An up to date global picture of Galactic spiral arms was given by Hou & Han (2014) with more than 1800 HII regions with known trigonometric, spectrophotometric or kinematic distances. Based on the distribution of known Galactic HII regions (Fig. 1 right), spiral arm segments are prominent in the first and fourth Galactic quadrants, implying the existence of a coherent spiral pattern of the Milky Way. Meanwhile, the HII region distribution is messy in some Galaxy regions, and the connections and continuity of arm segments in different Galactic quadrants are still unclear. Different models, e.g., three-arm and four-arm ones, are able to connect most HII regions (Hou & Han 2014). The classic four-arm picture originally proposed by Georgelin & Georgelin (1976) is unusually clean in comparison with modern HII region maps (e.g., Foster & Cooper 2010) and seems not to be the unique solution. The Galaxy's spiral structure is far from a closed subject. To explicitly uncover the entire picture, it is crucial to discover more weak and distant HII regions (e.g., Anderson et al. 2015), and reduce distance errors.

2.2 Neutral Atomic Hydrogen

Neutral atomic hydrogen (21 cm line) is ubiquitous in the Milky Way. The well defined HI gas disk is suggested to extend to about 35 kpc from the GC. Structures at multiple scales are present in the HI disk, from a small scale, e.g., filaments, bubbles, shells and spurs, to a large scale, such as warped, flared features and also spiral arms. The HI gas can be mapped throughout the entire Galaxy with the HI 21-cm line, providing a key probe to study the structure and dynamics of the Milky Way (e.g., see Dickey & Lockman 1990; Kalberla & Kerp 2009).

Soon after the discovery of the Galactic HI 21-cm line (Ewen & Purcell 1951), HI surveys were used to study the large-scale spiral structure. Christiansen & Hindman (1952) found two separate long features over a considerable range of Galactic longitudes in the $l-v$ diagram, suggesting the possible existence of spiral arms. Afterwards, early HI surveys were extended to a larger portion of the Galactic disk, and the observed HI (l - b -

v) data were converted to neutral atomic gas distributions in the Galactic plane (e.g., van de Hulst et al. 1954; Kerr et al. 1957; Westerhout 1957; Oort et al. 1958; Bok 1959; Weaver 1970) using velocity field models to derive the kinematic distances (e.g., Schmidt 1956), usually with an assumption of circular rotation. Prominent features in their results are arm-like segments extending from $R \sim 3$ kpc to $R > 10$ kpc. Since then, studies on the Galactic spiral structure were no longer confined to the vicinity of the Sun by the optical method (Morgan et al. 1952, 1953), but extended to almost the entire Galactic disk.

Along with the significant progresses, debates continue about maps of the HI distribution, primarily about the inner Galaxy regions (Simonson 1970). Even with almost identical data, derived HI maps of the inner Galaxy show discrepancies in the number and position of spiral arms (Kerr 1969; Weaver 1970). Major causes are large uncertainties in the kinematic distances of HI gas. Although Galactic HI primarily has circular rotation, random and non-circular motions could be significant, as large as $\lesssim 10$ km s⁻¹ or $< 5\%$ of the rotational velocity (Lockman 2002). The velocity crowding² can also be significant. Kinematic distance ambiguity makes the situation even worse. Deviations from circular rotation will cause systematic distortions in the kinematic distances, and hence the derived HI distribution maps may not be reliable. On the other hand, Burton (1971) pointed out that the observed HI profiles can be much better explained by velocity fields including both pure circular rotation and streaming motions than simply assuming a pure circular rotation, which suggested that the streaming motions predicted by density-wave theory can mimic or mask large density differences. It would be difficult to construct a true HI density map from the observed HI profiles. Up to now, evidence for a spiral structure from HI density distribution is still unclear for the inner Galaxy (Lockman 2002; Kalberla & Kerp 2009). For the outer Galaxy regions, however, it is easier to map the HI distribution, because there is no kinematic distance ambiguity. The sketch map of the main HI features obtained by Kerr (1969) and Weaver (1970) only showed a few points of disagreement, where the Carina Arm, Perseus Arm and Outer Arm in the first Galactic quadrant were presented. McClure-Griffiths et al. (2004) identified a new distant HI spiral arm in the fourth Galactic quad-

rant, which can be traced for over 70° in the $l - v$ diagram and probably is an extension of the Outer Arm in the fourth Galactic quadrant. By analyzing the combined Leiden-Argentine-Bonn all-sky HI survey data (Kalberla et al. 2005), Levine et al. (2006) constructed a perturbed surface density map of HI gas in the outer Galactic disk. The four non-axisymmetric spiral arm segments can be traced out to about 25 kpc from the GC. A more recent HI map in the outer Galaxy is constructed by identifying intensity peaks along each line of sight (Koo et al. 2017). Besides the HI emission data, evidence of spiral arms in the outer Galaxy regions has also been seen in the HI absorption measurements towards numerous continuum sources in the Galactic plane (e.g., Strasser et al. 2007; Dickey et al. 2009).

In general, observations of the HI distribution confine the spiral morphology and kinematics of the Galaxy, yet the spiral pattern has not been well established. Compared with young stellar objects and molecular gas, HI gas traces a much larger extent of the Galactic disk.

2.3 Molecular Gas

Molecular gas constitutes important components of the interstellar medium (ISM) in the Milky Way. The highly condensed region of molecular gas forms molecular clouds with different sizes and mass scales, and they are the birthplaces of young stars. Their distributions and kinematics represent the gas response to the Galaxy's gravitational potential, tracing the gaseous spiral arms. The spiral structure also plays a role in many processes involved in molecular gas evolution, such as large-scale spiral shock, cloud-cloud collisions, hydrodynamic instabilities, stellar feedback and magnetic fields (e.g., Dobbs & Baba 2014).

As we reside in the Milky Way, its molecular gas content could be surveyed in detail both with high sensitivity and resolution. Many observational efforts have been made to construct large-scale CO maps of the Galaxy (e.g., Burton & Gordon 1978; Cohen et al. 1980; Dame et al. 1987, 2001; Zhang et al. 2014b; Sun et al. 2015, 2017; Du et al. 2016, 2017). To explore the spiral structure with CO data, three different methods are widely used:

- **Spatial distributions of molecular clouds.**

Molecular clouds are vast assemblies of molecular gas and the birthplaces of dense molecular clumps and young stars. From the rich data set of CO surveys, a large number of isolated molecular clouds has been identified,

² The radial velocity remains almost constant over a long line of sight (e.g., Simonson 1970; Lockman 2002).

which have proven to be good tracers of Galaxy spiral arms. Using $^{12}\text{CO}(1-0)$ survey data from the Columbia 1.2 m millimeter telescope in New York (Cohen et al. 1980), Dame et al. (1986) identified 26 GMCs. The GMC distributions in the Galactic plane are found to resemble those of HII regions (Myers et al. 1986), and three segments of spiral arms, especially the Sagittarius Arm which is clear and continuous, are delineated in the first Galactic quadrant. Similar results were then confirmed by Solomon & Rivolo (1989) with 440 molecular clouds identified from observations of $^{12}\text{CO}(1-0)$, and also by Roman-Duval et al. (2009) with 750 molecular clouds identified from a $^{13}\text{CO}(1-0)$ survey using the Five College Radio Astronomy Observatory (FCRAO) 14 m telescope (also see Heyer & Dame 2015). In the southern sky, with a replica of the Columbia 1.2 m millimeter telescope in Chile, Cohen et al. (1985) surveyed the southern Milky Way and identified 37 molecular clouds in the Carina Arm. The famous Sagittarius-Carina Arm was then delineated with unprecedented clarity, which extends from the first to the fourth Galactic quadrants, more than 30 kpc in length (Grabelsky et al. 1988). In the fourth Galactic quadrant, some molecular clouds located in the Crux Arm and the Norma Arm were identified by Bronfman (1992). When the CO surveys further extended to the second and third Galactic quadrants, more molecular clouds were identified (e.g., Digel 1991; Sodroski 1991; May et al. 1997; Heyer et al. 2001; García et al. 2014). Some of them are located in the far outer Galaxy (e.g., Mead & Kutner 1988; Digel et al. 1990; Carpenter et al. 1990; Brand & Wouterloot 1994; Sun et al. 2015, 2017), even more than 20 kpc from the Sun (Dame & Thaddeus 2011; Sun et al. 2017). These known GMCs (mass $> 10^4 M_{\odot}$) were collected by Hou & Han (2014) from literature; more than 1200 GMCs have distances provided, mostly kinematic distances. More complete catalogs of Galactic molecular clouds were recently given by analyzing the classic whole-Galaxy CO maps of Dame et al. (2001). Rice et al. (2016) presented a catalog of 1064 high-mass molecular clouds (outer Galaxy: $M_{\text{clouds}} > 3 \times 10^3 M_{\odot}$; inner Galaxy: $M_{\text{clouds}} > 3 \times 10^4 M_{\odot}$) using a dendrogram-based decomposition. Miville-Deschênes et al. (2017) identified 8107 molecular clouds using a hierarchical cluster identification method, shown in Figure 2, including the results of the distant CO molecular clouds in the outer and far outer Galaxy found by Sun et al. (2015, 2017) and Du

et al. (2016, 2017) from the Milky Way Imaging Scroll Painting project³.

The major spiral arm segments traced by GMCs can be identified, i.e., in the first Galactic quadrant: the Scutum Arm, the Sagittarius Arm, the Perseus Arm, the Outer Arm and even beyond the Outer Arm (Outer+1 Arm), which is probably an extension of the Scutum-Crux-Centaurus Arm (Dame & Thaddeus 2011; Sun et al. 2015, 2017); in the fourth Galactic quadrant: the Carina Arm, the Centaurus Arm and the Norma Arm. In the second and third Galactic quadrants, consecutive arm-like features traced by GMCs are unexplained, probably due to the long-known velocity anomaly associated with the Perseus Arm (e.g., Foster & Cooper 2010). Although molecular clouds are good tracers of the global picture of spiral structure, only kinematic distances are available for the majority of known molecular clouds, which have large errors (e.g., see Ramón-Fox & Bonnell 2018). Large distance uncertainties of molecular clouds precluded making a true three-dimensional (3D) map of the Milky Way with sufficient accuracy to trace its spiral structure.

- **Deconvolution of the CO survey data cube.**

Rather than through the identifications of molecular clouds, the spatial distributions of molecular gas in the Milky Way could be constructed directly from the CO survey data cube, which are instructive to understand the global spiral structure, and also highly useful for understanding diffuse Galactic gamma-ray emission (e.g., Hunter et al. 1997) and the propagation and properties of cosmic rays (e.g., Jóhannesson et al. 2018). To interpret the observed properties of diffuse gamma-ray emissions, Hunter et al. (1997) constructed a surface density map of molecular gas from CO surveys (Dame et al. 1987). Based on the whole-Galaxy CO maps of Dame et al. (2001), Nakanishi & Sofue (2006) created a 3D distribution map of molecular gas throughout the Galactic plane, and some concentrated areas of molecular gas are visible and consistent with the features shown in the molecular cloud map (see Fig. 2), but not as clear as those traced by HII regions. The gas concentrations probably are related to the major spiral arm segments as shown in figure 14 of Nakanishi & Sofue (2006). After that, Nakanishi & Sofue (2016) presented a new combination of HI and H₂ surface density maps with similar methods. Pohl et al. (2008) used a gas-flow model to derive a model of the spatial distribution of molecular gas in

³ <http://www.radioast.nsd.cn/mwisp.php>

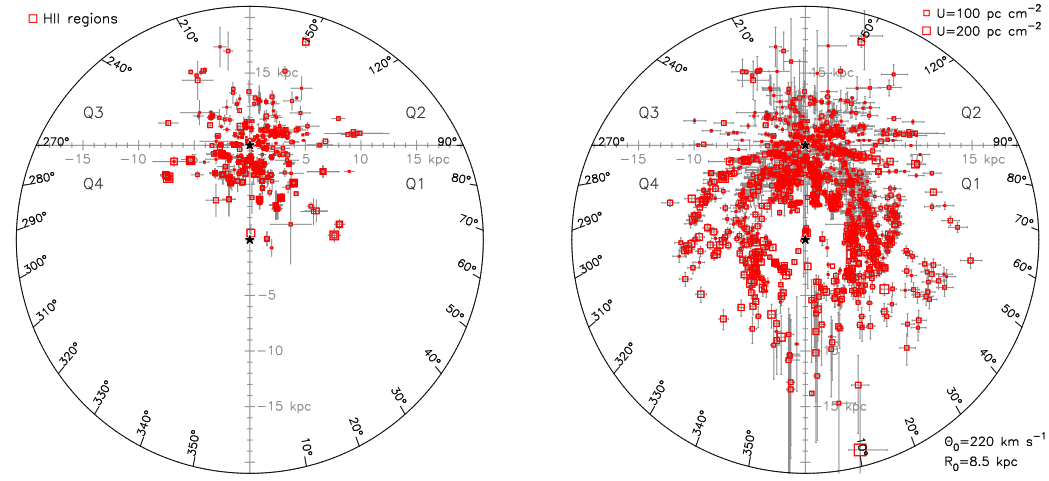


Fig. 1 *Left*: Distribution of HII regions (red) with known spectrophotometric distances. *Right*: Distribution of Galactic HII regions (red) with spectroscopic distances or kinematic distances. The symbol size is proportional to the excitation parameters. The IAU standard $R_0 = 8.5$ kpc and $\Theta_0 = 220$ km s $^{-1}$, and the standard solar motions together with a flat rotation curve are adopted in deriving the kinematic distances. Two *black stars* indicate the locations of the Sun ($x = 0.0$ kpc, $y = 8.5$ kpc) and the GC ($x = 0.0$ kpc, $y = 0.0$ kpc). Q1 to Q4 indicate the four Galactic quadrants. Position uncertainties are indicated by error bars (gray). Galactic longitudes in degrees are also marked in the plots. The HII region data are taken from Hou & Han (2014).

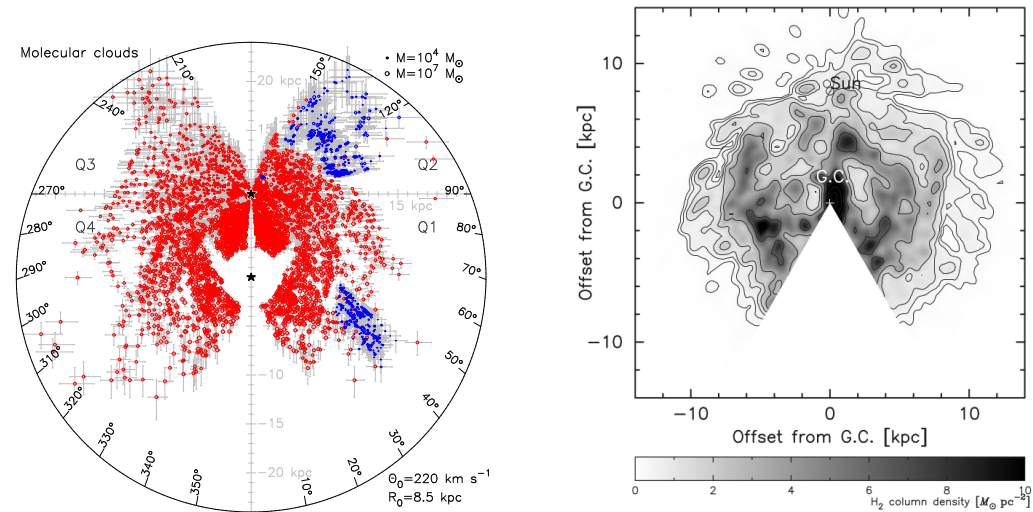


Fig. 2 *Left*: Distribution of molecular clouds in the Galactic disk, the data of which are from Miville-Deschênes et al. (2017, red) and the Milky Way Imaging Scroll Painting project (Sun et al. 2015, 2017; Su et al. 2016; Du et al. 2016, 2017, blue). The symbol size is proportional to the mass of molecular clouds. The IAU standard $R_0 = 8.5$ kpc and $\Theta_0 = 220$ km s $^{-1}$ and the standard solar motions together with a flat rotation curve are adopted in deriving the kinematic distances. Two *black stars* indicate the locations of the Sun ($x = 0.0$ kpc, $y = 8.5$ kpc) and the GC ($x = 0.0$ kpc, $y = 0.0$ kpc). Q1 to Q4 indicate the four Galactic quadrants. Position uncertainties are indicated by error bars (gray). Galactic longitudes in degrees are marked in the plots. *Right*: Spatial distribution of molecular gas in the Galaxy derived by deconvolution of the CO survey data cube (Dame et al. 2001) by Nakanishi & Sofue (2006). Adapted with permission from Professors Nakanishi, H. & Sofue, Y.

the Milky Way from the CO survey maps of Dame et al. (2001), rather than simply assuming a pure circular rotation picture. They found a concentration of mass along the Galactic bar, and at the ends of the bar, two spiral arms emerge. However, the evidences for other spi-

ral arms are not strong as shown from the deconvolution map of surface density (fig. 6 of Pohl et al. 2008).

The global 3D distributions of molecular gas could be re-constructed by deconvolution of the survey data cube $T_b(l, b, v)$ of CO. This method depends on the adopted model of the Galaxy velocity field (e.g., circular

or non-circular), which is basic to derive the kinematic distances of molecular gas. It also depends on the near-and-far or kinematic distance ambiguity. From the current results, spiral arm features shown by this method are not clear or continuous. It seems impossible to determine the global spiral structure from this method alone.

• **Modeling the observed longitude-velocity maps of CO.** From the CO survey (l - b - v) data toward the Galaxy, the longitude-velocity ($l-v$) diagram can be created by integrating emission over latitude (e.g., Dame et al. 1987, 2001). The large-scale distributions and kinematics of molecular clouds in the Galaxy are embedded in the emission features shown in the $l-v$ map (fig. 3 of Dame et al. 2001), which indicate the concentrations of stars and interstellar gas, tracing some remarkable structures such as the spiral arms, the 3-kpc arms, the Galactic Molecular Ring and arm tangencies. To interpret and transform the observed $l-v$ map to a 3D distribution of gas, a model of gas flow is required. Many numerical efforts have been made (e.g., see Dobbs & Baba 2014; Pettitt et al. 2014). Englmaier & Gerhard (1999) presented a model for gas dynamics in the inner Galactic plane. Their best model leads to a four-armed spiral structure and reproduces the observed directions towards five arm tangencies. Fux (1999) modeled gas dynamics in the Galactic disc with a 3D N -body simulation. The gas flow in the model can reproduce some major features in the CO $l-v$ map, but only at specific times, suggesting a transient nature of the Galaxy's spiral arms. Rodriguez-Fernandez & Combes (2008) modeled the gas flow by including the nuclear bar constrained by 2MASS data. Their simulations reproduced the major spiral arms, the near and far 3-kpc arms, and interpreted the Galactic Molecular Ring as the inner parts of spiral arms rather than an actual ring. Baba et al. (2010) used an N -body and hydrodynamical simulation to model the CO $l-v$ map, in which multi-phase ISM, star formation and supernova feedback were considered. They qualitatively reproduced the large-scale emission features of the CO $l-v$ diagram and also clumpy structures. In a face-on view of their best gas flow model, the Milky Way looks more like a multiple-arm or flocculent galaxy rather than a grand design spiral galaxy. Pettitt et al. (2014) used smoothed particle hydrodynamics to simulate gas flow in the Milky Way by assuming a grand design spiral (four-armed or two-armed). They found that it is possible to reproduce the major features shown in the $l-v$ map of CO, but neither four-armed nor two-armed models can reproduce all of the observed features simultaneously.

Then, Pettitt et al. (2015) took a different approach by modeling the stellar distribution with many discrete N -body particles rather than a continuous gravitational potential. Their best fitted models can match the observed CO $l-v$ map much better than previous work and favor a four-armed structure, but the spiral arms are dynamic and transient. Generally, the precise global spiral pattern and the formation mechanism cannot be uniquely determined from current gas flow models of the Milky Way.

2.4 Open Clusters

The open clusters (OCs) have a wide range of ages, from a few million years to more than ten billion years. The young OCs are too young to migrate far from their birth locations. For old OCs, they gradually drift away from their birthplace and move to inter-arm regions. Becker (1963, 1964) first studied the relation between OCs and spiral arms using a sample of 156 OCs with photometric distances. He pointed out that the distribution of OCs with the earliest spectral type between O and B2 probably followed three spiral arm segments in the vicinity of the Sun, and resembled the distribution of nearby HII regions, while the distribution of older OCs with spectral type between B3 and F did not indicate spiral arm segments and seemed to be random. These conclusions were confirmed by Becker & Fenkart (1970) and Fenkart & Binggeli (1979) with larger samples of OCs. With a sample of 212 OCs, Dias & Lépine (2005) showed that the OCs with ages up to about 1.2×10^7 yr remain in parts of the Perseus Arm, the Local Arm and the Sagittarius-Carina Arm; those with ages ~ 20 Myr are leaving the spiral arms and filling the interarm regions; for clusters older than 30 Myr, the spiral or clumpy-like structure has disappeared in their distribution. Therefore, it is generally believed that young OCs are tracers of Galactic spiral arms. However, from the distributions of about 120 open clusters with age $< 10^{7.5}$ yr, Lynga (1982) suggested these features seem like three clumpy-like concentrations or complexes, rather than associations to extended spiral arms. Janes & Adler (1982) and Janes et al. (1988) independently obtained a similar conclusion from a larger sample (> 400 young OCs). They suggested that the distributions of OCs look like some clumps or short arm segments, with no spiral pattern at all. At present, the number of known open clusters has significantly increased to more than 3000 (see e.g., Dias et al. 2002; Kharchenko et al. 2013; Schmeja et al. 2014; Loktin & Popova 2017; He et al. 2018). As shown in Figure 3, a

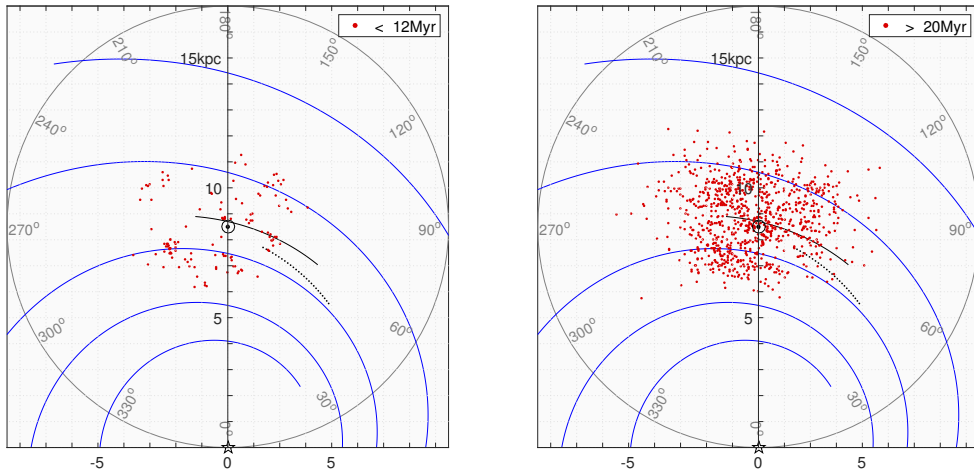


Fig. 3 *Left*: Distribution of young open clusters with age < 12 Myr. *Right*: Distribution of older open clusters with age > 20 Myr. Two *black stars* indicate the locations of the Sun ($x = 0.0$ kpc, $y = 8.5$ kpc) and the GC ($x = 0.0$ kpc, $y = 0.0$ kpc). Galactic longitudes in degrees are also marked in the plots. The cluster data are taken from He et al. (2018). The background is the spiral arm model obtained by Hou & Han (2014) through fitting the Galactic distributions of known HII regions with a polynomial-logarithmic spiral arm model, except the Local Arm, whose parameters are adopted from the recent work of Xu et al. (2016). From top to bottom, they are the Outer Arm, the Perseus Arm, the Local Arm, the Sagittarius-Carina Arm, the Scutum-Crux-Centaurus Arm and the Norma Arm.

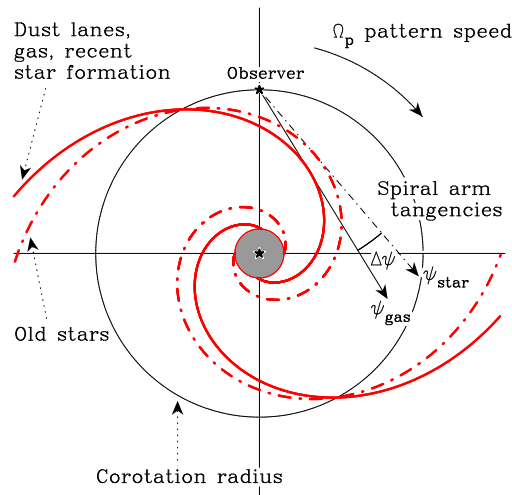


Fig. 4 Schematic of spiral arm tangencies for gas (ψ_{gas}) and old stars (ψ_{star}), which are indicated by the density peaks and/or irregular terminal velocities near the tangency points of ideal spiral arms; also shown are the relative positions between the spiral arms traced by gas and old stellar components according to the predictions of quasi-stationary density wave theory (e.g., Roberts 1969). Adapted with permission from Hou & Han (2015).

majority of them is located within about 3 kpc from the Sun. The 126 OCs with age less than 12 Myr are concentrated in parts of the Perseus Arm, the Local Arm and the Sagittarius-Carina Arm. On the contrary, the old OCs seem to be distributed randomly. Due to the extinction of interstellar dust, it would be difficult to identify distant young OCs. At present, it seems not possible to infer the global spiral structure of the Milky Way from OCs alone.

2.5 Arm Tangencies in the Inner Galaxy

As shown by face-on spiral galaxies (e.g., M101, Fig. 6), spiral arms appear to be long and thin features in the distributions of interstellar gas and stars. These large-scale structures originate near the galaxy center and extend to the far outer edge, normally approximated by logarithmic form (e.g., Honig & Reid 2015). As shown in Figure 4, tangencies of spiral arms are expected for an observer

inside the host galaxy. As to our Milky Way, the arm tangencies have long been known as one of the best pieces of evidence for spiral arms in the inner Galaxy, and provide useful observational constraints to spiral structure models (e.g., Burton & Shane 1970; Georgelin & Georgelin 1976; Ortiz & Lepine 1993; Englmaier & Gerhard 1999; Cordes & Lazio 2002; Russeil 2003; Benjamin 2008; Hou & Han 2014). In addition, the possible displacements of arm tangencies for different components (e.g., gas and stars) can be used to constrain the formation mechanisms of spiral arms in the Milky Way (e.g., Vallée 2014; Hou & Han 2015).

Arm tangencies have been identified by a number of research works from the survey of molecular gas, atomic gas, ionized gas, and young and old stellar components in the Galactic disk. A recent compilation was given by Vallée (2014, 2016), which ignores the different definitions of arm tangencies in references. The derived arm tangencies by different definitions may be different by about half of the arm width even from the same observation data. To properly measure the arm tangencies, a consistent definition and multi-wavelength survey data should be considered together.

- For baryons in the ISM (e.g., ionized gas, atomic gas and molecular gas), the tangencies of spiral arms have been measured:

- (1) by the bump features or condensed emissions appearing in the (l, v) diagrams of HI (e.g., Burton & Shane 1970; Robinson et al. 1984), CO (e.g., Grabelsky et al. 1987; Englmaier & Gerhard 1999), HII regions (e.g., Lockman 1989; Englmaier & Gerhard 1999) and methanol masers (e.g., Caswell et al. 2011);

- (2) by the excess velocity features shown in the terminal velocity curve of HI (e.g., Burton 1971; Shane 1972; McClure-Griffiths & Dickey 2007), CO (e.g., Clemens 1985; Alvarez et al. 1990) and HII regions (e.g., Rohlfs et al. 1986), which were interpreted as the result of streaming motions along the spiral arms, and/or large internal motions of the cloud complexes;

- (3) by the solid-body like kinematic features in the smoothed rotation curve of CO (Luna et al. 2006), which meet the peaks in the gas surface density curve and the valleys in the shear and vorticity curve;

- (4) by the local peaks or enhancement in the integrated emissions of CO, HI, radio recombination lines (RRLs) or thermal radio continuum over latitude/velocity with Galactic longitude (e.g., Beuermann et al. 1985; Bronfman et al. 1989; Steiman-Cameron et al. 2010); and by local maxima in the integrated number counts

of HII regions, 6.7 GHz methanol masers, dense molecular clumps or pulsars, over Galactic latitude and plotted against longitude (e.g., Cordes & Lazio 2002; Hou & Han 2015);

- (5) from the best spiral arm models fitted to the projected distributions of spiral tracers (such as HI, molecular clouds, HII regions and HMSFR masers) in the Galactic plane (e.g., Russeil 2003; Hou et al. 2009), or from the models fitted to the (l, v) diagram (e.g., Englmaier & Gerhard 1999). The derived arm tangencies are suggested to be less confident than the above four methods.

- As to the stellar components in the inner Galaxy, it is still difficult to measure radial velocities for a large number of distant stars due to interstellar dust extinction. The arm tangencies were commonly identified by local maxima shown in the integrated number counts of near-infrared (NIR) or far-infrared (FIR) point sources, or the integrated NIR or FIR emissions against Galactic longitudes (e.g., Drimmel 2000; Drimmel & Spergel 2001; Benjamin 2008). The interstellar extinction seems to not significantly influence the measured longitudes of arm tangencies from the survey data of old stars (Benjamin 2008; Hou & Han 2015). It should be mentioned that the identified arm tangencies by measuring the local maxima deviate from the true density maxima of matter (gas or stars) near the arm tangencies by shifting to the inner side due to the effect of integration along the line of sight. The discrepancy is probably small, i.e., less than about $1^\circ \sim 2^\circ$ in longitude (Drimmel 2000; Hou & Han 2015).

We emphasize that there are pitfalls in the above methods used to identify arm tangencies. Velocity crowding, including streaming motions (e.g., Burton 1973), can result in “bump” features in the (l, v) diagram. The concentrations of individual clouds, star-forming regions or old stars can produce local maxima in the integrated number count plots and the integrated emission plots against Galactic longitudes. The nearby clouds, star-forming regions or old stars could be wrongly recognized as longitudinal concentrations of farther objects and then be misinterpreted as arm tangencies. In addition, observations of interstellar gas or old stars towards arm tangencies could be complicated by dust extinction effects. Observations of small distant objects suffer from the beam dilution effect. In order to properly identify arm tangencies for a better understanding of the Milky Way’s spiral structure, a consistent definition and multiwavelength surveys of different Galactic components should

Table 1 Galactic longitudes of spiral arm tangencies for old stars and interstellar gas, identified from multiwavelength observational data (see Hou & Han 2015).

Component	Near 3 kpc North (°)	Scutum (°)	Sagittarius (°)	Carina (°)	Centaurus (°)	Norma (°)	Near 3 kpc South (°)
Old stars	27.0	32.6	55.0*	–	307.5	–	338.3
Interstellar gas	24.4*	30.7	49.4	283.8	305.5, 311.2	328.1	337.0*

Notes: *, the measured arm tangencies have lower confidence, as the corresponding local maxima features are not present in all of the investigated datasets.

be considered together, because the problems discussed above may be present in one or two data sets, but not in all datasets. A careful re-evaluation of arm tangencies with more survey data of interstellar gas and stars would be useful.

Such kind of work has recently been done with the method of identifying local maxima in the longitude plots of source number counts for GLIMPSE/2MASS sources, HII regions, 6.7 GHz methanol masers, dense clumps and in the plots of integrated emissions for RRLs, HI, ^{12}CO and ^{13}CO (Hou & Han 2015). The arm tangencies identified for different gas components in the ISM, i.e., HII regions, methanol masers, CO gas, dense molecular clumps and HI gas, appear at nearly the same Galactic longitudes. The arm tangencies for GLIMPSE and 2MASS old stars also appear at nearly the same longitudes. The results are summarized in Table 1 for comparisons with spiral structure models of the Milky Way. By using other definitions, e.g., excess velocity features in the terminal velocity curve, a systematic re-evaluation of arm tangencies with modern survey data has not yet been done. Such investigations may provide some insight into uncovering the possible displacements of arm tangencies between different gas components, which was found by Vallée (2014), but not confirmed by Hou & Han (2015). In addition, the tangencies for some arm segments are still uncertain, e.g., the Sagittarius Arm tangency for old stars, the near and far 3-kpc Arm tangencies for gas (see Table 1), as the corresponding local maxima features, were not found in all of the studied data sets, and deserve more attention with survey data of stars and gas in the near future.

3 VLBI AND GAIA ASTROMETRY

Over the past decade, the astrometric accuracy of VLBI has improved dramatically. Pioneering work measured the trigonometric parallaxes and proper motions to masers associated with HMSFR W3OH and obtained an accuracy of $10 \mu\text{as}$ (Xu et al. 2006), allowing us to per-

form precise distance measurements to objects at the GC and beyond, extending to the outer edge of the Galaxy. This is a landmark in this field (Binney 2006; Caswell 2012). Currently, relative positions between sources separated by about one degree are being measured with accuracies of a few μas (Honma et al. 2007; Reid et al. 2009a; Zhang et al. 2013; Sanna et al. 2017). With this accuracy, trigonometric parallaxes can be obtained accurately throughout the Milky Way. These techniques have been applied to VLBI networks like the NRAO Very Long Baseline Array (VLBA) in the USA, the European VLBI Network (EVN) in Europe and China, or the VLBI Exploration of Radio Astrometry (VERA) array in Japan (Reid & Honma 2014).

The astrometric satellite *Gaia* is expected to significantly augment our knowledge about Galactic structure and space motions. With the most accurate astrometric parameters of the youngest O stars and masers, for the first time, the spiral structure in all four quadrants has been delineated clearly in unprecedented detail (Xu et al. 2018). The revealed Galactic spiral patterns make a clear sketch of nearby spiral arms, especially in the fourth quadrant where maser parallax measurements are absent.

In addition to distances, *Gaia* also yields excellent measurements of secular proper motions, with accuracies of $\approx 1 \text{ km s}^{-1}$. Combining radial velocities with proper motions (and distances) yields full 3D velocities, relative to the motion of the Sun. Thus, through this measurement, one may also be able to determine the full kinematics in the Milky Way, which can accurately define its associated rotation curve (Brunthaler et al. 2011; Honma et al. 2012; Reid et al. 2014). Therefore, the current astrometry can provide an excellent opportunity to map our Galaxy in great detail, yielding the precise geometry, Galactic fundamental parameters and 3D velocity field.

In this section, we review progress on spiral structures of the Milky Way made during the past decade relying on VLBI and *Gaia* astrometry. Meanwhile, we

present our own latest research results from astrometric measurements.

3.1 New Galactic Spiral Arms

Here we display the spiral structure revealed by O stars from *Gaia* DR2 and VLBI maser parallax measurements. Because some sources have considerable uncertainties (typically more than 20% and a few even more than 30%) in their parallaxes, which are comparable to the size of spacing between arms, only those with distance accuracies better than 15% are adopted. Collectively, 102 masers (Ando et al. 2011; Asaki et al. 2010; Bartkiewicz et al. 2008; Brunthaler et al. 2009; Choi et al. 2008, 2014; Hachisuka et al. 2006, 2009, 2015; Hirota et al. 2008; Honma et al. 2007, 2011; Immer et al. 2013; Kim et al. 2008; Kurayama et al. 2011; Menten et al. 2007; Moellenbrock et al. 2009; Moscadelli et al. 2009, 2011; Nagayama et al. 2011; Niinuma et al. 2011; Oh et al. 2010; Reid et al. 2009a,b; Rygl et al. 2010, 2012; Sandstrom et al. 2007; Sanna et al. 2009, 2012, 2014; Sato et al. 2008, 2010a,b, 2014; Shiozaki et al. 2011; Wu et al. 2014; Xu et al. 2006, 2009, 2011, 2013; Zhang et al. 2009, 2012b,a, 2013, 2014a) and 635 O stars (Xu et al. 2018) are listed in Tables 2 and 3 respectively.

In order to purify the O star sample that is truly capable of tracing spiral arms, we further eliminated those with peculiar motions in the direction perpendicular to the Galactic plane larger than 20 km s^{-1} and with a 3D velocity of more than 60 km s^{-1} , resulting in a total of 583 O stars. They are the youngest stars and their peculiar motions are relatively small, which means they are supposed to be located near their birthplaces. With a typical lifetime of 3 Myr (Weidner & Vink 2010), O5.0 III stars would move $\sim 0.2 \text{ kpc}$ from their birth places at a speed of 60 km s^{-1} . Because the width of spiral arms neighboring the Sun ranges from 0.2 to 0.4 kpc (Reid et al. 2014) and the lines of sight usually are not perpendicular to spiral arms, the remaining O stars are guaranteed to be located in their spiral arms.

As shown in Figure 5, the conjunctions of VLBI and *Gaia* parallax results are distributed in strips and clumps, meaning that they trace spiral arms, while the sources are relatively sparse indicating the gap between spiral arms. For the first time, these data fill in the whole sky, especially the previous gap from 240° to 360° along Galactic longitude. As expected, most O stars are gathered around the Sun within a radius of $\sim 3 \text{ kpc}$, while the masers, despite a relatively small number, are distributed much

more widely than the O stars, even over 10 kpc. In general, they reveal a clear spiral pattern, consisting of five obvious spiral arm segments. From top to bottom, they are part of the Outer Arm, the Perseus Arm, the Local Arm, the Sagittarius Arm and the Scutum Arm. These measurements strongly support the existences of spiral arms in the Milky Way Galaxy.

Masers are assigned to arms based on their coincidence in Galactic longitude and velocities in the Local Standard of Rest frame (V_{LSR}) with CO and HI $l-v$ emission features (Reid et al. 2014; Xu et al. 2016), while for O stars, because of their large peculiar motions, the method based on $\log(r) - \theta$ information is the same as Hou & Han (2014) for HII regions and GMCs. Here, r represents the distance to the GC, and θ starts from the positive x -axis and increases counterclockwise.

Although there are only four maser sources in a long longitude distribution, from $l \approx 74^\circ$ to 190° , they outline an arc shape, i.e., part of an arm segment in the Outer Arm. The Perseus Arm has a large number of HMSFRs. Between $l \approx 90^\circ$ and 210° , masers and O stars mix well, firmly tracing the arm segment. On one end, the maser data extend to $l \approx 45^\circ$, but there is a lack of masers and O stars between $l \approx 45^\circ$ and 90° in this arm. On the other end, the O stars extend the arm segment to $l \approx 255^\circ$. The Local Arm is the nearest spiral arm to the Sun. Considering all relevant optical and radio data available at the time, Georgelin & Georgelin (1976) concluded that the Local Arm was a “spur” or a secondary spiral feature, because the density of star forming regions appeared to be significantly less than that of other major arms in the Milky Way. However, Xu et al. (2013) found a larger number of star forming regions in this arm, some of which were thought to be in the Perseus Arm, suggesting that the Local Arm is a major spiral structure. The Local Arm stretches approximately from $l \approx 70^\circ$, past the Sun, upward slightly and at $l \approx 240^\circ$ bends down to l over 270° with one branch (see shadow area) touching the Perseus Arm at around $l \approx 200^\circ$. In spite of a higher abundance of high-mass stars, this branch resembles the spur that links the Local Arm and the Sagittarius Arm discovered by Xu et al. (2016). Unlike the vast sources in the Perseus and Local Arms, there are not too many masers located in the Sagittarius Arm. Most of the masers are concentrated between $l \approx 0^\circ$ and 30° . Only a few masers extend to $l \approx 45^\circ$. On the other end, O stars stretch into the fourth quadrant at about $l \approx 285^\circ$. Masers located in the Scutum Arm are confined between $l \approx 0^\circ$ and 30° . On the other end, the O stars may extend

Table 2 Parallaxes and Proper Motions of Masers

Name	R.A. ($^{\circ}$)	Dec. ($^{\circ}$)	π (mas)	μ_x (mas yr $^{-1}$)	μ_y (mas yr $^{-1}$)	v_{LSR} (km s $^{-1}$)	Spiral Arm
(1)	(2)	(3)	(4)	(5)	(6)	(7)	(8)
L 1287	09.1975	63.4841	1.077 ± 0.039	-0.86 ± 0.11	-2.29 ± 0.56	-23 ± 5	Loc
G122.01–07.08	11.2433	55.7799	0.460 ± 0.020	-3.70 ± 0.50	-1.25 ± 0.50	-50 ± 5	Per
G123.06–06.30	13.1008	56.5620	0.421 ± 0.022	-2.69 ± 0.31	-1.77 ± 0.29	-29 ± 3	Per
G123.06–06.30	13.1030	56.5640	0.355 ± 0.030	-2.79 ± 0.62	-2.14 ± 0.70	-30 ± 5	Per
G134.62–02.19	35.7155	58.5865	0.413 ± 0.017	-0.49 ± 0.35	-1.19 ± 0.33	-39 ± 5	Per
...							

Notes: Column (1) gives the Galactic source name; Cols. (2) and (3) are Right Ascension and Declination (J2000), respectively; Cols. (4) to (6) give the parallax and proper motion in the eastward ($\mu_x = \mu_{\alpha} \cos \delta$) and northward directions ($\mu_y = \mu_{\delta}$), respectively; Col. (7) lists local standard of rest (LSR) velocity. The same as Reid et al. (2014), Col. (8) indicates the spiral arm in which it resides. The full table is available in the electronic attachment (<http://www.raa-journal.org/docs/Supp/ms4260table2.dat>).

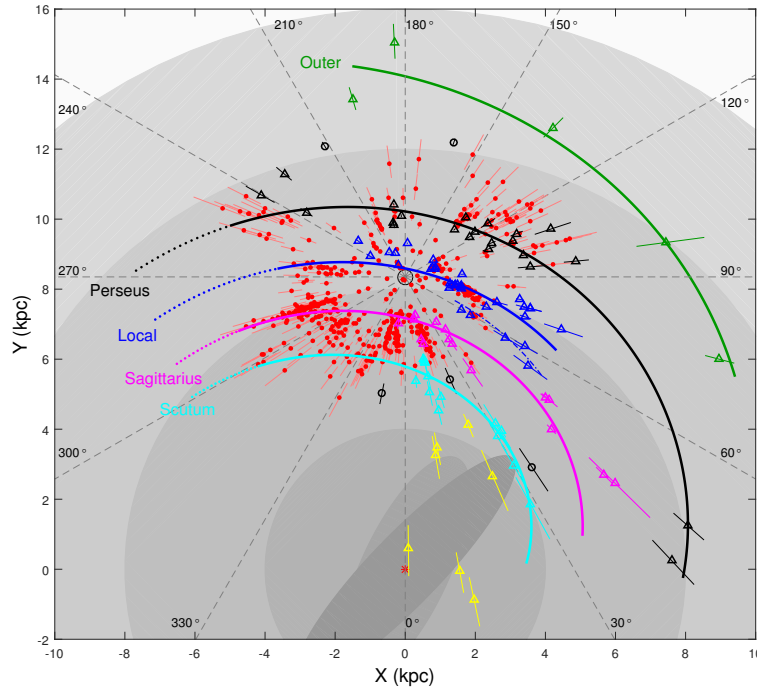


Fig. 5 Up to date face-on view of the spiral arms determined from parallaxes of masers (*triangles*) and O stars (*red circles*). The formal parallax uncertainties of the sources shown here are better than 15%. *Solid curved lines* depict the log-periodic spiral fitting, while *dotted lines* are generated by extrapolating the log-periodic spirals. Here $R_0 = 8.35$ kpc (see Sect. 3.2).

the Scutum Arm from $l \approx 0^{\circ}$ to $l \approx 300^{\circ}$ into the fourth quadrant.

Figure 5 shows many more possible branches/spurs. Besides the Local spur that links the Local Arm and the Sagittarius Arm (Xu et al. 2016) and links the Local Arm and the Perseus Arm at around $l \approx 200^{\circ}$, other spurs are identifiable. Between the Sagittarius Arm and Scutum Arm there are a few possible spurs that cannot be conclusively confirmed due to large distance uncertainties. Near $l \approx 280^{\circ}$, it looks like one branch of the Sagittarius Arm going upward and connecting to the Local Arm. Although current parallax data are inadequate to clearly

describe the entire Galactic structure, based on present results, our Galaxy may have many sub-structures in addition to its major arms. This suggests that our Galaxy is quite different from a pure grand design spiral galaxy with well-defined, two- or four-major arms being the dominant, such as M51, although a pure grand design morphology is more popular. Our Milky Way largely resembles an external galaxy, the Pinwheel Galaxy (M101) (Fig. 6).

The pitch angle is an indicator of the tightness of spiral arms. Usually, a logarithmic model is used to fit pitch angles because spiral arms of galaxies crudely

Table 3 Parallaxes and Proper Motions of O Stars

Name	<i>Gaia</i> DR2 ID	R.A.	Dec.	π	μ_x	μ_y	v_{LSR}	Spectral	Spiral
(1)	(2)	($^{\circ}$) (3)	($^{\circ}$) (4)	(mas) (5)	(mas yr $^{-1}$) (6)	(mas yr $^{-1}$) (7)	(km s $^{-1}$) (8)	Type (9)	Arm (10)
ALS 13375	528594342521399168	0.4453	67.5070	1.016 \pm 0.031	-1.57 \pm 0.04	-1.77 \pm 0.04		O9.5V	Loc
ALS 13379	528570015826682496	0.5429	67.4089	0.928 \pm 0.035	-1.61 \pm 0.05	-2.04 \pm 0.05	-0.6	O7V	Loc
ALS 6006	429470895385555456	0.9896	61.1036	0.289 \pm 0.032	-0.85 \pm 0.05	-1.74 \pm 0.05	-20.2 \pm 2	O9.7Iab	Per
ALS 6009	429927879906030336	1.0158	62.2219	0.295 \pm 0.037	-1.40 \pm 0.06	-1.72 \pm 0.05	-36.6 \pm 0.3	O8Iabf	Per
ALS 6014	528409143531333376	1.0673	66.3491	0.917 \pm 0.038	-1.15 \pm 0.05	-4.19 \pm 0.05		O9	Loc
...									

Notes: Column (1) is the name of Alma luminous star (ALS); Col. (2) is the unique source identifier in *Gaia* DR2; Cols. (3) and (4) are Barycentric Right Ascension (R.A.) and Declination (Dec.), respectively. Columns (5) to (7) give the parallax and proper motion in the eastward ($\mu_x = \mu_\alpha \cos \delta$) and northward directions ($\mu_y = \mu_\delta$), respectively. Column (8) lists local standard of rest (LSR) velocity; Col. (9) is the specific spectral subtype of the O stars; Col. (10) indicates the spiral arm in which it resides. In *Gaia* DR2, the reference epoch is J2015.5. The full table is available in the electronic attachment (<http://www.raa-journal.org/docs/Supp/ms4260table3.dat>).

agree with a logarithmic form (Kennicutt 1981; Honig & Reid 2015). Following the method of Xu et al. (2013), we fitted masers and O stars together with arm segments, adopting a log-periodic spiral defined by

$$\ln(R/R_{\text{ref}}) = -(\beta - \beta_{\text{ref}}) \tan \psi, \quad (1)$$

where R is the Galactocentric radius at a Galactocentric azimuth β (defined as 0 toward the Sun and increasing clockwise) for an arm with radius R_{ref} at reference azimuth β_{ref} and pitch angle ψ . To search for the optimized values of each parameter, we minimized the factor

$$Z = \frac{1}{\sum W_i} \sum W_i \sqrt{(x_i - x_t)^2 + (y_i - y_t)^2}, \quad (2)$$

where W_i is the weight. We simply assigned the weight factor $W_o = 1$ for the O stars and the weight factor $W_m = 10$ for masers, because the amount of masers is much smaller but they are distributed much more widely; x_i and y_i are the Cartesian coordinates of a spiral tracer; x_t and y_t are the coordinates of the nearest point from the fitted spiral arms to the tracer. The Minuit package (James & Roos 1975) was adopted to minimize the factor Z . The best fitting logarithmic model of a spiral arm shows that the pitch angle of the major arms ranges from 9 $^{\circ}$ to 19 $^{\circ}$ (Table 4). This is characteristic of major arms in Sb-Sc type galaxies (Kennicutt 1981).

3.2 Fundamental Galactic Parameters

In this section, we investigate Galactic Parameters R_0 and Θ_0 , solar motions and rotation curves using both *Gaia* O star and VLBI astrometric data. Such a study can examine the consistency between *Gaia* and VLBI techniques and the quality of current *Gaia* DR2 data. We used the Bayesian model fitting approach of Reid et al. (2014), based on observations of the radial velocity in the heliocentric frame, V_{helio} , and the proper motion in Galactic

Table 4 Spiral Arm Characteristics

Arm	β_{ref}	R_{ref}	ψ
(1)	($^{\circ}$) (2)	(kpc) (3)	($^{\circ}$) (4)
Scutum	-3.1	5.9 \pm 0.1	18.7 \pm 0.8
Sagittarius	-0.0	7.2 \pm 0.1	13.5 \pm 0.5
Local	2.2	8.5 \pm 0.1	11.5 \pm 0.5
Perseus	-11.8	10.6 \pm 0.1	9.0 \pm 0.1

Notes: Columns (2) and (3) give the reference Galactocentric azimuth and the fitted radius at that azimuth respectively. Column (4) is the spiral arm pitch angle, indicating how tightly wound the spiral is.

coordinates (μ_l, μ_b). The posteriori probability density functions (PDFs) of models were estimated with Markov chain Monte Carlo (MCMC) trials which were sampled with the Metropolis-Hastings algorithm.

In Section 3.1, the structure of the spiral arm was derived from 102 masers and 635 O stars, however, to estimate Galactic parameters R_0 and Θ_0 with kinematic models, we need to construct a subset by removing sources with extremely large peculiar motions. For O stars, we firstly estimated their peculiar motions with a prior model, the Univ model from table 5 of Reid et al. (2014), and subsequently derived the standard deviation (std) of peculiar motions (U_s, V_s, W_s), which are (15, 13, 10) km s $^{-1}$, respectively. Here U_s, V_s and W_s are velocity components toward the GC, in the direction of Galactic rotation, and toward the North Galactic Pole in a Galactocentric reference frame, respectively. As W_s is less likely to be affected by the asymmetric spiral gravitational potential, here we adopt the std of W_s , 10 km s $^{-1}$ as the typical value of random motions for O stars. Then O stars with peculiar motions larger than 30 km s $^{-1}$ (3 times the random motion) in any direction along U_s, V_s and W_s components are excluded, which selects 291 O stars. With the same criterion, we selected 95 masers.



Fig. 6 The galaxy M101. The Milky Way is likely to be this type of galaxy with abundant branches/spurs. Adapted with permission from Dr. R. Jay GaBany.

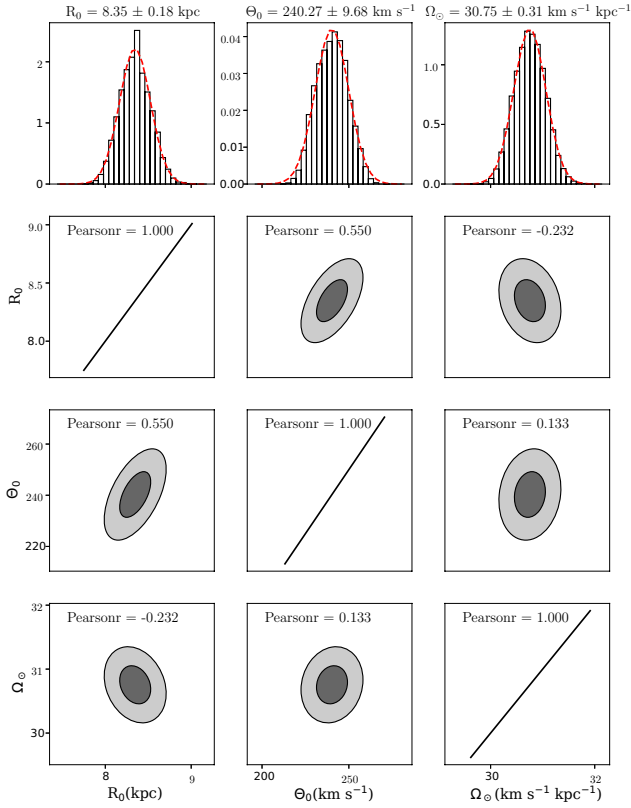


Fig. 7 The marginalized (upper row panels) and joint (lower 3-row panels) posteriori PDFs for R_0 , Θ_0 and Ω_\odot , estimated based on 291 O stars and 95 masers. (1) Upper panels, the red lines are Gaussian fittings of the marginalized PDFs; (2) Lower panels, the deep and light grey areas denote 68% and 95% probabilities of joint PDFs. Pearson correlation coefficients are labeled in the tops of panels.

Consequently, our analysis was based on the 291 O stars and 95 masers.

In Reid et al. (2014), the proper motion and Doppler velocity weights were given by $w(\mu) = \sqrt{\sigma_\mu^2 + \sigma_{\text{vir}}^2}/d^2$ and $w(V_{\text{helio}}) = \sqrt{\sigma_v^2 + \sigma_{\text{vir}}^2}$, where a random (virial) motion of $\sigma_{\text{vir}} = 5 \text{ km s}^{-1}$ was adopted. In this study, for the 95 maser data, we used the same weighting strategy as Reid et al. (2014). For the 291 O star datasets, when calculating the observables V_{helio} and (μ_l, μ_b) , we found the formal error of these observables is very small, at a level of $\sim 1 \text{ km s}^{-1}$. On the other hand, the stds of peculiar motions (U_s, V_s, W_s) are $(15, 13, 10) \text{ km s}^{-1}$, which can be the typical value of random (virial) motions. Thus, in practice, we adopted a (virial) motion of $\sqrt{(15^2 + 13^2)/2} = 14 \text{ km s}^{-1}$ in μ_l and V_{helio} directions and virial dispersion of 10 km s^{-1} in the μ_b direction for O stars. With this weighting strategy, we achieved a reduced chi-square of ~ 1.0 , indicating such a weighting strategy is reasonable.

As to the choice of the rotation curve, by fitting Galactic parameters and solar motions with different types of rotation curves and comparing the posterior statistic (χ^2) of these fittings, Reid et al. (2014) concluded that the Persic96 universal rotational curve (Persic et al. 1996) is slightly better than other models, such as the two-order polynomial, Brand & Blitz (1993)'s (BB) power-law (Brand & Blitz 1993), and Clemens's rotation curves (Clemens 1985). Here we made similar comparisons of four types of rotation curves: 1st-order polynomial, 2nd-order polynomial, BB's power-law and Persic96 universal rotational curve. We merged the 291 O stars and 95 masers into a single dataset, which is used to fit the rotation curves, and the results are listed in Table 5. In summary, we found the same conclusion as Reid et al. (2014) that the universal rotational curve is better than other types of rotation curves.

Finally, we estimated parameters including R_0 , Θ_0 , rotation curve parameters a_2/a_3 , ($a_1 = \Theta_0$), solar motions $U_\odot, V_\odot, W_\odot$ and average peculiar motions $\overline{U}_s, \overline{V}_s$. When adopting the universal rotation curve, we found $R_0 = 8.35 \pm 0.18 \text{ kpc}$ and $\Theta_0 = 240 \pm 10 \text{ km s}^{-1}$, which are very consistent with the values ($R_0 = 8.31 \pm 0.16 \text{ kpc}$, $\Theta_0 = 241 \pm 8 \text{ km s}^{-1}$) given by Reid et al. (2014) at a 1σ level. The angular speed $\Omega_\odot = \Theta_0/R_0$ of the Sun with respect to the GC is $30.75 \pm 0.31 \text{ km s}^{-1} \text{ kpc}^{-1}$, which is also consistent with Reid et al. (2014), $\Omega_\odot = 30.57 \pm 0.43 \text{ km s}^{-1} \text{ kpc}^{-1}$, at a 1σ level, and consistent with the proper motion measurement of Sgr A* (Reid &

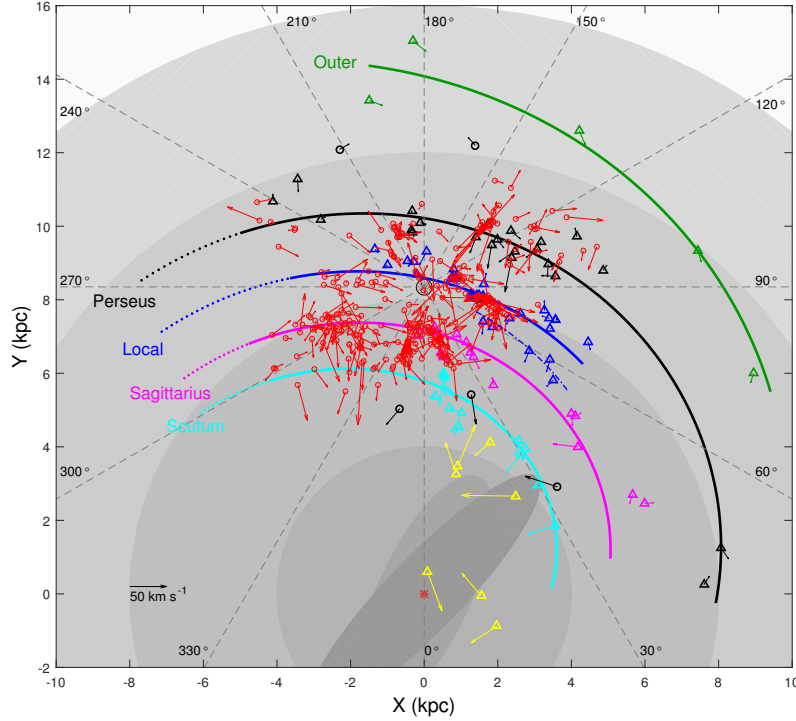


Fig. 8 Peculiar motion vectors of O stars (*open circles*) and masers (*open triangles*). A motion scale of 50 km s^{-1} is indicated in the bottom left corner of the panel. The background is the same as in figure 1 of Reid et al. (2014). The Galaxy is viewed from the North Galactic Pole, it rotates clockwise and the Sun is at $(X = 0.0 \text{ kpc}, Y = 8.35 \text{ kpc})$.

Brunthaler 2004), $\Omega_{\odot} = 29.45 \pm 0.15 \text{ km s}^{-1} \text{ kpc}^{-1}$ at a 2σ level.

To investigate the quality of the *Gaia* DR2 data, we estimated R_0 and Θ_0 with only the 291 O star data. Here we fixed the rotation curve parameters and solar motions, taking into account the limited Galactic coverage of O-star data. The fitting results are presented in the last column of Table 5. The R_0 and Θ_0 values estimated with O-star data are consistent with maser-O star combined results but with larger uncertainties. In addition, the pure O-star dataset yields a very large correlation coefficient 0.970. In summary, currently, maser astrometric data with better accuracy and wider Galactic distribution are better than *Gaia* DR2 data in estimation of R_0 and Θ_0 . In the future, with more measurements of maser parallaxes and better *Gaia* datasets, we expect that the fundamental Galactic parameters could be determined better.

3.3 Galactic Dynamics

With distances, proper motions and radial velocities, one has full 3D velocity information. In this section, we calculate 3D velocities for these sources and demonstrate

their peculiar motions (with respect to the Galactocentric reference frame). 3D velocities are calculated straightforwardly with linear speeds on the celestial sphere (obtained with proper motions and distances) and radial velocities. Subsequently, we estimate their peculiar (non-circular) motions by subtracting the effect of Galactic rotation and peculiar motions of the Sun.

We estimated peculiar motions of O stars following Reid et al. (2009c), using updated Galactic parameters of 240 km s^{-1} for the Galactic rotation speed, Θ_0 , at a distance of 8.35 kpc to the GC, R_0 , and solar motion parameters of $U_{\odot} = 13.3 \text{ km s}^{-1}$, $V_{\odot} = 17.0 \text{ km s}^{-1}$ and $W_{\odot} = 8.6 \text{ km s}^{-1}$ from this work (“universal” rotation curve model). Because velocities for bright stars are not available in *Gaia* DR2, the velocities of O stars are taken from Reid (2003).

Since sources near the GC may have large non-circular motions, due to the great gravitational potential of the Galactic bar, we removed the sources within a radius of 4 kpc from the GC. In addition, we eliminated those with peculiar motions in the direction perpendicular to the Galactic plane, larger than 40 km s^{-1} and with a 3D velocity of more than 90 km s^{-1} , resulting in a total of 318 O stars and 94 masers. The results of the pecu-

Table 5 Rotation Curve Fitting Results

	R_0 (kpc)	Θ_0 (km s ⁻¹)	r_{R_0, Θ_0}	a_2	a_3	U_\odot	V_\odot	W_\odot	\overline{U}_s	\overline{V}_s	N_{dof}	N_{source}	χ^2
						(km s ⁻¹)							
1-Poly	8.40±0.19	242±10	0.539	-0.1±4.3	—	14.3±2.6	15.7±9.0	8.6±0.6	5.8±2.7	0.6±9.0	1150	386	1230.0
2-Poly	8.38±0.19	241±9	0.576	1.7±4.0	-14.8±11.0	13.9±2.7	14.6±7.5	8.6±0.6	5.3±2.8	0.1±7.5	1149	386	1225.4
BB	8.38±0.17	241±9	0.491	-0.02±0.01	—	14.5±2.7	15.3±8.0	8.6±0.6	5.8±2.7	0.1±8.0	1150	386	1226.9
Univ	8.35±0.18	240±10	0.550	0.88±0.07	1.39±0.13	13.3±2.6	17.0±8.0	8.6±0.6	4.8±2.6	2.6±8.0	1149	386	1211.6
Univ [†]	8.57±0.63	239±18	0.970	0.88	1.39	13.3	17.0	8.6	3.4±1.1	3.7±1.1	869	291	916.4

Notes: [†], fit R_0 , Θ_0 , \overline{U}_s and \overline{V}_s using 291 O stars with solar motions and rotation curve fixed.

Table 6 Mean Peculiar Motions

Source Type	\overline{U}	ΔU	\overline{V}	ΔV	\overline{W}	ΔW
	(km s ⁻¹)					
Masers	4.9	11.9	1.6	10.0	2.0	8.2
O stars	8.1	19.6	8.6	16.8	3.5	10.9

Notes: \overline{U}_s , \overline{V}_s and \overline{W}_s are velocity components toward the GC in the direction of Galactic rotation and toward the North Galactic Pole average peculiar motions, respectively. The mean peculiar motions of both the O stars and the masers are small, indicating the motions are random. However, O stars have much larger std (ΔU , ΔV) than that of masers.

liar motions of the sources are listed in Table 4, while the peculiar motions are shown in Figure 8.

One can see that the average velocities of O stars are larger than those of masers, especially in the direction of Galactic rotation. O stars rotate faster, >8 km s⁻¹, than the rotational speed, while the maser’s movement approximates the rotation speed. On the other hand, it is noted that although their peculiar motions are generally random, toward the GC and the direction of Galactic rotation, the O stars have much larger std than that of the masers. Here the gravitational potential of the Galactic bar is small, so the peculiar motions are intrinsic, suggesting that O stars and masers may be located in different physical environments. Because these masers are associated with HMSFRs, when the high-mass stars should be bound to their native molecular clouds tightly, some of the O stars have perhaps picked up peculiar motions from the dispersal of gas/dust from their birth clouds to move out there.

We further investigate the number of O stars associated with their natal molecular clouds. Based on the archived CO data⁴ with a typical root mean square (rms) noise level of about 0.3 K, we found 207 O stars have CO observations and 103 of them have associated ¹³CO emission within 10′, indicating that about 50% (1–103/207) of O stars may have left their natal molecular clouds already. In addition, we found a large average deviation of ~ 16 km s⁻¹ between remaining O stars and the

CO molecular clouds. Since CO emission is widespread in the Galactic plane, in order to avoid the ambiguity caused by multiple peaks in CO spectra, we only use the CO data with a single peak. Such a deviation indeed suggests that the O stars and masers live in different physical environments.

4 PROSPECTS

4.1 Limitations of Present Facilities

Although the VLBI technique can achieve an angular accuracy of a few μ as, it is not easy to fully reconstruct the Galactic spiral arms because of many limiting factors. At present, the astrometric errors are large due to the sensitivity of current equipments, atmospheric effects and lack of stations in the southern hemisphere. The poor sensitivity of telescopes, such as the VLBA, results in limitation of available sources. Because phase-referenced observations involve two angularly-close sources, i.e., a phase calibrator (quasar) and a target source (maser, pulsar, etc), the switching time must be very short, especially at high frequencies, usually a minute or less to achieve phase connection across multiple scans. Therefore, only the sources with strong intensities can be used for parallax measurements with the VLBA. In practice, 12 GHz methanol and 22 GHz water masers that are roughly stronger than 5 Jy are useful. In this case, in total only about 300 of both kinds of masers are available whereas their total number is over 3000. The switching time is a little bit longer for 6.7 GHz methanol masers, so the flux

⁴ <http://www.radioast.nsd.cnr/english/index.php>

density threshold is ~ 2 Jy. In this case, approximately 400 6.7 GHz methanol masers are useful (also in consideration of compactness of sources), while the expected total number of such masers is over 3000. Therefore, finishing these scientific aims requires improved sensitivity to the present equipments.

At present, atmospheric effects dominate the astrometric errors. The in-beam calibration method could greatly remove atmospheric effects. However, low sensitivity and small field of view of present instruments make it hard to find in-beam calibrators. Due to atmospheric effects, systematic errors are proportional to the separation angle between targets and their calibrators. For example, there are several calibrators for the HMSFR W3OH. Among them, one calibrator has a separation of less than 1° , which leads to an accuracy of about $15 \mu\text{as}$, while another calibrator doubles in angle, resulting in the uncertainty almost doubling (Xu et al. 2006). Therefore, to obtain highly accurate astrometry, it is necessary to use highly sensitive telescopes and many more calibrators close to targets.

In addition, there are relatively few stations in the southern hemisphere. In order to improve the $u-v$ coverage of interferometry and image quality, both southern and northern hemisphere telescopes are needed. At present, only the Australia Long Baseline Array (LBA) is being tested to measure the parallaxes toward some star forming regions in the southern hemisphere. However, with its limited numbers of antennas and short baselines, it may not have competitive advantages in this project.

4.2 Highly Accurate Astrometry with the SKA

The Square Kilometre Array (SKA) will change this situation revolutionarily. Although exact types and numbers of antennas have not been determined yet, one square kilometer of collecting area is the final aim. SKA-VLBI sensitivity would be expected to achieve a sensitivity of μJy flux, roughly two orders of magnitude better than now. This should significantly increase the ability to detect weak sources. Therefore, it can find many more targets and calibrators with accurate positions because sources with high signal-to-noise ratios can greatly improve their position accuracies. On the other hand, the antennas composing the SKA are not large, about 15-m in diameter, so it has a relatively large field of view.

The superior sensitivity and large field of view will ensure detecting more targets and calibrators within the same beam. For baselines over 1000 km, the systematic

errors are dominated by delays introduced by Earth's atmosphere and ionosphere. For highly accurate astrometry, it is crucial to remove the residual tropospheric and ionospheric effects, in particular for low-frequency observations. In general, there are two ways: (1) measuring the tropospheric delay above each antenna during observations. By observing large numbers of extragalactic sources spread over the sky to measure broadband delays (Reid et al. 2009a), the ionospheric delays can be partially removed by applying a global ionospheric model derived from GPS measurements; (2) using calibrators with a small angular separation from targets. Sources as weak as a few μJy should be useful for the SKA-VLBI observations. Statistically, the weaker the calibrator is, the higher the chance it can be found near the target. Using adjacent (in-beam calibration is optimal) and multiple calibrators helps reduce systematic errors owing to time variation in the atmosphere and calibrator structure. In this way, a good imaging quality would be produced and the astrometric accuracy will be roughly equal to the resolution divided by the dynamic range of the image. Therefore, together with current VLBI arrays, one can obtain an accuracy of a few μJy for positions and $\sim 1 \mu\text{Jy}$ for parallaxes at high frequencies (>5 GHz), which ensures parallax and proper motion measurements throughout the whole Milky Way.

5 SUMMARY

There is neither general agreement on the number of arms nor on their locations and orientations in early models of spiral structure because typical uncertainties in distances are comparable to the spacing between arms. With the most accurate astrometric parameters of the youngest O-type stars and parallax-measured masers, for the first time, the spiral structure in all four quadrants is delineated clearly. The revealed Galactic spiral patterns make a clear sketch of nearby spiral arms. In addition, the best values of R_0 and Θ_0 were estimated. However, the progress on VLBI astrometry is largely limited by low sensitivity of present facilities and large residual atmospheric effects. The superior sensitivity and large field of view of the SKA will allow us to map objects with unprecedented accuracy throughout the entire Galaxy.

Acknowledgements This work was sponsored by the MOST (Grant No. 2017YFA0402701), the NSFC (Grant Nos. 11873019, 11673066 and 11503033), the CAS (Grant No. QYZDJ-SSW-SLH047), the Youth Innovation Promotion Association of CAS

and is also supported by the Key Laboratory for Radio Astronomy, CAS and the Open Project Program of the Key Laboratory of FAST, NAOC, CAS. This work has made use of data from the ESA mission *Gaia* (<https://www.cosmos.esa.int/Gaia>), processed by the *Gaia* DPAC, <https://www.cosmos.esa.int/web/Gaia/dpac/consortium>. Funding for the DPAC has been provided by national institutions, in particular the institutions participating in the *Gaia* Multilateral Agreement.

References

- Alexander, S. 1852, *AJ*, 2, 95
- Alvarez, H., May, J., & Bronfman, L. 1990, *ApJ*, 348, 495
- Anderson, L. D., Armentrout, W. P., Johnstone, B. M., et al. 2015, *ApJS*, 221, 26
- Anderson, L. D., Bania, T. M., Balsler, D. S., & Rood, R. T. 2012, *ApJ*, 754, 62
- Ando, K., Nagayama, T., Omodaka, T., et al. 2011, *PASJ*, 63, 45
- Asaki, Y., Deguchi, S., Imai, H., et al. 2010, *ApJ*, 721, 267
- Avedisova, V. S. 1985, *Soviet Astronomy Letters*, 11, 185
- Baba, J., Saitoh, T. R., & Wada, K. 2010, *PASJ*, 62, 1413
- Bartkiewicz, A., Brunthaler, A., Szymczak, M., van Langevelde, H. J., & Reid, M. J. 2008, *A&A*, 490, 787
- Becker, W. 1963, *ZAp*, 57, 117
- Becker, W. 1964, in *IAU Symposium*, 20, *The Galaxy and the Magellanic Clouds*, ed. F. J. Kerr, 16
- Becker, W., & Fenkart, R. B. 1970, in *IAU Symposium*, 38, *The Spiral Structure of our Galaxy*, ed. W. Becker & G. I. Kontopoulos, 205
- Benjamin, R. A. 2008, in *Astronomical Society of the Pacific Conference Series*, 387, *Massive Star Formation: Observations Confront Theory*, ed. H. Beuther, H. Linz, & T. Henning, 375
- Beuermann, K., Kanbach, G., & Berkhuijsen, E. M. 1985, *A&A*, 153, 17
- Binney, J. J. 2006, *Science*, 311, 44
- Bok, B. J. 1959, *The Observatory*, 79, 58
- Bok, B. J., Hine, A. A., & Miller, E. W. 1970, in *IAU Symposium*, 38, *The Spiral Structure of our Galaxy*, ed. W. Becker & G. I. Kontopoulos, 246
- Brand, J., & Blitz, L. 1993, *A&A*, 275, 67
- Brand, J., & Wouterloot, J. G. A. 1994, *A&AS*, 103, 503
- Bronfman, L. 1992, in *Astrophysics and Space Science Library*, 180, *The Center, Bulge, and Disk of the Milky Way*, ed. L. Blitz, 131
- Bronfman, L., Alvarez, H., Cohen, R. S., & Thaddeus, P. 1989, *ApJS*, 71, 481
- Brunthaler, A., Reid, M. J., Menten, K. M., et al. 2009, *ApJ*, 693, 424
- Brunthaler, A., Reid, M. J., Menten, K. M., et al. 2011, *Astronomische Nachrichten*, 332, 461
- Burton, W. B., & Shane, W. W. 1970, in *IAU Symposium*, 38, *The Spiral Structure of our Galaxy*, ed. W. Becker & G. I. Kontopoulos, 397
- Burton, W. B. 1971, *A&A*, 10, 76
- Burton, W. B. 1973, *PASP*, 85, 679
- Burton, W. B., & Gordon, M. A. 1978, *A&A*, 63, 7
- Carpenter, J. M., Snell, R. L., & Schloerb, F. P. 1990, *ApJ*, 362, 147
- Caswell, J. L., & Haynes, R. F. 1987, *A&A*, 171, 261
- Caswell, J. L., Fuller, G. A., Green, J. A., et al. 2011, *MNRAS*, 417, 1964
- Caswell, J. L. 2012, arXiv:1210.0978
- Choi, Y. K., Hirota, T., Honma, M., et al. 2008, *PASJ*, 60, 1007
- Choi, Y. K., Hachisuka, K., Reid, M. J., et al. 2014, *ApJ*, 790, 99
- Christiansen, W. N., & Hindman, J. V. 1952, *Australian Journal of Scientific Research A Physical Sciences*, 5, 437
- Clemens, D. P. 1985, *ApJ*, 295, 422
- Cohen, R. S., Cong, H., Dame, T. M., & Thaddeus, P. 1980, *ApJ*, 239, L53
- Cohen, R. S., Grabelsky, D. A., May, J., et al. 1985, *ApJ*, 290, L15
- Cordes, J. M., & Lazio, T. J. W. 2002, astro-ph/0207156
- Crampton, D., & Georgelin, Y. M. 1975, *A&A*, 40, 317
- Dame, T. M., Elmegreen, B. G., Cohen, R. S., & Thaddeus, P. 1986, *ApJ*, 305, 892
- Dame, T. M., Ungerechts, H., Cohen, R. S., et al. 1987, *ApJ*, 322, 706
- Dame, T. M., Hartmann, D., & Thaddeus, P. 2001, *ApJ*, 547, 792
- Dame, T. M., & Thaddeus, P. 2011, *ApJ*, 734, L24
- Dias, W. S., Alessi, B. S., Moitinho, A., & Lépine, J. R. D. 2002, *A&A*, 389, 871
- Dias, W. S., & Lépine, J. R. D. 2005, *ApJ*, 629, 825
- Dickey, J. M., & Lockman, F. J. 1990, *ARA&A*, 28, 215
- Dickey, J. M., Strasser, S., Gaensler, B. M., et al. 2009, *ApJ*, 693, 1250
- Digel, S., Bally, J., & Thaddeus, P. 1990, *ApJ*, 357, L29
- Digel, S. W. 1991, *Molecular clouds in the distant outer galaxy*, PhD thesis, Harvard University, Cambridge, MA.
- Dobbs, C., & Baba, J. 2014, *PASA*, 31, e035
- Downes, D., Wilson, T. L., Bieging, J., & Wink, J. 1980, *A&AS*, 40, 379
- Drimmel, R. 2000, *A&A*, 358, L13
- Drimmel, R., & Spergel, D. N. 2001, *ApJ*, 556, 181
- Du, X., Xu, Y., Yang, J., et al. 2016, *ApJS*, 224, 7
- Du, X., Xu, Y., Yang, J., & Sun, Y. 2017, *ApJS*, 229, 24
- Englmaier, P., & Gerhard, O. 1999, *MNRAS*, 304, 512

- Ewen, H. I., & Purcell, E. M. 1951, *Nature*, 168, 356
- Fenkart, R. P., & Binggeli, B. 1979, *A&AS*, 35, 271
- Fich, M., & Blitz, L. 1984, *ApJ*, 279, 125
- Foster, T., & Brunt, C. M. 2015, *AJ*, 150, 147
- Foster, T., & Cooper, B. 2010, in *Astronomical Society of the Pacific Conference Series*, 438, *The Dynamic Interstellar Medium: A Celebration of the Canadian Galactic Plane Survey*, ed. R. Kothes, T. L. Landecker, & A. G. Willis, 16
- Fux, R. 1999, *A&A*, 345, 787
- Gaia Collaboration, Prusti, T., de Bruijne, J. H. J., et al. 2016, *A&A*, 595, A1
- Gaia Collaboration, Brown, A. G. A., Vallenari, A., et al. 2018, *A&A*, 616, A1
- García, P., Bronfman, L., Nyman, L.-Å., Dame, T. M., & Luna, A. 2014, *ApJS*, 212, 2
- Georgelin, Y. M., & Georgelin, Y. P. 1976, *A&A*, 49, 57
- Grabelsky, D. A., Cohen, R. S., Bronfman, L., & Thaddeus, P. 1988, *ApJ*, 331, 181
- Grabelsky, D. A., Cohen, R. S., Bronfman, L., Thaddeus, P., & May, J. 1987, *ApJ*, 315, 122
- Hachisuka, K., Brunthaler, A., Menten, K. M., et al. 2009, *ApJ*, 696, 1981
- Hachisuka, K., Brunthaler, A., Menten, K. M., et al. 2006, *ApJ*, 645, 337
- Hachisuka, K., Choi, Y. K., Reid, M. J., et al. 2015, *ApJ*, 800, 2
- Han, J. L., Manchester, R. N., van Straten, W., & Demorest, P. 2018, *ApJS*, 234, 11
- He, Z. H., Xu, Y., Zhang, B., et al. 2018, submitted
- Heyer, M. H., Carpenter, J. M., & Snell, R. L. 2001, *ApJ*, 551, 852
- Heyer, M., & Dame, T. M. 2015, *ARA&A*, 53, 583
- Hirota, T., Ando, K., Bushimata, T., et al. 2008, *PASJ*, 60, 961
- Honig, Z. N., & Reid, M. J. 2015, *ApJ*, 800, 53
- Honma, M., Bushimata, T., Choi, Y. K., et al. 2007, *PASJ*, 59, 889
- Honma, M., Hirota, T., Kan-Ya, Y., et al. 2011, *PASJ*, 63, 17
- Honma, M., Nagayama, T., Ando, K., et al. 2012, *PASJ*, 64, 136
- Hou, L. G., Han, J. L., & Shi, W. B. 2009, *A&A*, 499, 473
- Hou, L. G., & Han, J. L. 2014, *A&A*, 569, A125
- Hou, L. G., & Han, J. L. 2015, *MNRAS*, 454, 626
- Hunter, S. D., Bertsch, D. L., Catelli, J. R., et al. 1997, *ApJ*, 481, 205
- Immer, K., Reid, M. J., Menten, K. M., Brunthaler, A., & Dame, T. M. 2013, *A&A*, 553, A117
- James, F., & Roos, M. 1975, *Computer Physics Communications*, 10, 343
- Janes, K., & Adler, D. 1982, *ApJS*, 49, 425
- Janes, K. A., Tilley, C., & Lynga, G. 1988, *AJ*, 95, 771
- Jóhannesson, G., Porter, T. A., & Moskalenko, I. V. 2018, *ApJ*, 856, 45
- Kalberla, P. M. W., Burton, W. B., Hartmann, D., et al. 2005, *A&A*, 440, 775
- Kalberla, P. M. W., & Kerp, J. 2009, *ARA&A*, 47, 27
- Kennicutt, Jr., R. C. 1981, *AJ*, 86, 1847
- Kerr, F. J. 1969, *ARA&A*, 7, 39
- Kerr, F. J., Hindman, J. V., & Carpenter, M. S. 1957, *Nature*, 180, 677
- Kharchenko, N. V., Piskunov, A. E., Schilbach, E., Röser, S., & Scholz, R.-D. 2013, *A&A*, 558, A53
- Kim, M. K., Hirota, T., Honma, M., et al. 2008, *PASJ*, 60, 991
- Koo, B.-C., Park, G., Kim, W.-T., et al. 2017, *PASP*, 129, 094102
- Kurayama, T., Nakagawa, A., Sawada-Satoh, S., et al. 2011, *PASJ*, 63, 513
- Levine, E. S., Blitz, L., & Heiles, C. 2006, *Science*, 312, 1773
- Lockman, F. J. 1989, *ApJS*, 71, 469
- Lockman, F. J. 2002, in *Astronomical Society of the Pacific Conference Series*, 276, *Seeing Through the Dust: The Detection of HI and the Exploration of the ISM in Galaxies*, ed. A. R. Taylor, T. L. Landecker, & A. G. Willis, 107
- Loktin, A. V., & Popova, M. E. 2017, *Astrophysical Bulletin*, 72, 257
- Luna, A., Bronfman, L., Carrasco, L., & May, J. 2006, *ApJ*, 641, 938
- Lynga, G. 1982, *A&A*, 109, 213
- May, J., Alvarez, H., & Bronfman, L. 1997, *A&A*, 327, 325
- McClure-Griffiths, N. M., & Dickey, J. M. 2007, *ApJ*, 671, 427
- McClure-Griffiths, N. M., Dickey, J. M., Gaensler, B. M., & Green, A. J. 2004, *ApJ*, 607, L127
- Mead, K. N., & Kutner, M. L. 1988, *ApJ*, 330, 399
- Menten, K. M., Reid, M. J., Forbrich, J., & Brunthaler, A. 2007, *A&A*, 474, 515
- Miville-Deschênes, M.-A., Murray, N., & Lee, E. J. 2017, *ApJ*, 834, 57
- Moellenbrock, G. A., Claussen, M. J., & Goss, W. M. 2009, *ApJ*, 694, 192
- Morgan, W. W., Sharpless, S., & Osterbrock, D. 1952, *AJ*, 57, 3
- Morgan, W. W., Whitford, A. E., & Code, A. D. 1953, *ApJ*, 118, 318
- Moscadelli, L., Cesaroni, R., Rioja, M. J., Dodson, R., & Reid, M. J. 2011, *A&A*, 526, A66
- Moscadelli, L., Reid, M. J., Menten, K. M., et al. 2009, *ApJ*, 693, 406
- Myers, P. C., Dame, T. M., Thaddeus, P., et al. 1986, *ApJ*, 301, 398
- Nagayama, T., Omodaka, T., Nakagawa, A., et al. 2011, *PASJ*, 63, 23
- Nakanishi, H., & Sofue, Y. 2006, *PASJ*, 58, 847
- Nakanishi, H., & Sofue, Y. 2016, *PASJ*, 68, 5
- Niinuma, K., Nagayama, T., Hirota, T., et al. 2011, *PASJ*, 63, 9

- Oh, C. S., Kobayashi, H., Honma, M., et al. 2010, *PASJ*, 62, 101
- Oort, J. H. 1927, *Bull. Astron. Inst. Netherlands*, 3, 275
- Oort, J. H., Kerr, F. J., & Westerhout, G. 1958, *MNRAS*, 118, 379
- Ortiz, R., & Lepine, J. R. D. 1993, *A&A*, 279, 90
- Paladini, R., Davies, R. D., & De Zotti, G. 2004, *MNRAS*, 347, 237
- Persic, M., Salucci, P., & Stel, F. 1996, *MNRAS*, 281, 27
- Pettitt, A. R., Dobbs, C. L., Acreman, D. M., & Bate, M. R. 2015, *MNRAS*, 449, 3911
- Pettitt, A. R., Dobbs, C. L., Acreman, D. M., & Price, D. J. 2014, *MNRAS*, 444, 919
- Pohl, M., Englmaier, P., & Bissantz, N. 2008, *ApJ*, 677, 283
- Ramón-Fox, F. G., & Bonnell, I. A. 2018, *MNRAS*, 474, 2028
- Reed, B. C. 2003, *AJ*, 125, 2531
- Reid, M. J., & Brunthaler, A. 2004, *ApJ*, 616, 872
- Reid, M. J., Menten, K. M., Brunthaler, A., et al. 2009a, *ApJ*, 693, 397
- Reid, M. J., Menten, K. M., Zheng, X. W., Brunthaler, A., & Xu, Y. 2009b, *ApJ*, 705, 1548
- Reid, M. J., Menten, K. M., Zheng, X. W., et al. 2009c, *ApJ*, 700, 137
- Reid, M. J., & Honma, M. 2014, *ARA&A*, 52, 339
- Reid, M. J., Menten, K. M., Brunthaler, A., et al. 2014, *ApJ*, 783, 130
- Rice, T. S., Goodman, A. A., Bergin, E. A., Beaumont, C., & Dame, T. M. 2016, *ApJ*, 822, 52
- Roberts, W. W. 1969, *ApJ*, 158, 123
- Robinson, B. J., Manchester, R. N., Whiteoak, J. B., et al. 1984, *ApJ*, 283, L31
- Rodríguez-Fernández, N. J., & Combes, F. 2008, *A&A*, 489, 115
- Rohlf, K., Boehme, R., Chini, R., & Wink, J. E. 1986, *A&A*, 158, 181
- Roman-Duval, J., Jackson, J. M., Heyer, M., et al. 2009, *ApJ*, 699, 1153
- Rosse, T. E. O. 1850, *Philosophical Transactions of the Royal Society of London Series I*, 140, 499
- Russeil, D. 2003, *A&A*, 397, 133
- Rygl, K. L. J., Brunthaler, A., Reid, M. J., et al. 2010, *A&A*, 511, A2
- Rygl, K. L. J., Brunthaler, A., Sanna, A., et al. 2012, *A&A*, 539, A79
- Sandstrom, K. M., Peek, J. E. G., Bower, G. C., Bolatto, A. D., & Plambeck, R. L. 2007, *ApJ*, 667, 1161
- Sanna, A., Reid, M. J., Moscadelli, L., et al. 2009, *ApJ*, 706, 464
- Sanna, A., Reid, M. J., Dame, T. M., et al. 2012, *ApJ*, 745, 82
- Sanna, A., Reid, M. J., Menten, K. M., et al. 2014, *ApJ*, 781, 108
- Sanna, A., Reid, M. J., Dame, T. M., Menten, K. M., & Brunthaler, A. 2017, *Science*, 358, 227
- Sato, M., Hirota, T., Honma, M., et al. 2008, *PASJ*, 60, 975
- Sato, M., Hirota, T., Reid, M. J., et al. 2010a, *PASJ*, 62, 287
- Sato, M., Reid, M. J., Brunthaler, A., & Menten, K. M. 2010b, *ApJ*, 720, 1055
- Sato, M., Wu, Y. W., Immer, K., et al. 2014, *ApJ*, 793, 72
- Schmeja, S., Kharchenko, N. V., Piskunov, A. E., et al. 2014, *A&A*, 568, A51
- Schmidt, M. 1956, *Bull. Astron. Inst. Netherlands*, 13, 15
- Shane, W. W. 1972, *A&A*, 16, 118
- Shiozaki, S., Imai, H., Tafuya, D., et al. 2011, *PASJ*, 63, 1219
- Simonson, III, S. C. 1970, *A&A*, 9, 163
- Sodroski, T. J. 1991, *ApJ*, 366, 95
- Solomon, P. M., & Rivolo, A. R. 1989, *ApJ*, 339, 919
- Steiman-Cameron, T. Y., Wolfire, M., & Hollenbach, D. 2010, *ApJ*, 722, 1460
- Strasser, S. T., Dickey, J. M., Taylor, A. R., et al. 2007, *AJ*, 134, 2252
- Su, Y., Sun, Y., Li, C., et al. 2016, *ApJ*, 828, 59
- Sun, Y., Xu, Y., Yang, J., et al. 2015, *ApJ*, 798, L27
- Sun, Y., Su, Y., Zhang, S.-B., et al. 2017, *ApJS*, 230, 17
- Urquhart, J. S., Figura, C. C., Moore, T. J. T., et al. 2014, *MNRAS*, 437, 1791
- Vallée, J. P. 2014, *ApJS*, 215, 1
- Vallée, J. P. 2016, *ApJ*, 821, 53
- van de Hulst, H. C., Muller, C. A., & Oort, J. H. 1954, *Bull. Astron. Inst. Netherlands*, 12, 117
- Weaver, H. 1970, in *IAU Symposium*, 38, *The Spiral Structure of our Galaxy*, ed. W. Becker & G. I. Kontopoulos, 126
- Weidner, C., & Vink, J. S. 2010, *A&A*, 524, A98
- Westerhout, G. 1957, *Bull. Astron. Inst. Netherlands*, 13, 201
- Westpfahl, D. J. 1998, *ApJS*, 115, 203
- Wu, Y. W., Sato, M., Reid, M. J., et al. 2014, *A&A*, 566, A17
- Xu, Y., Reid, M. J., Zheng, X. W., & Menten, K. M. 2006, *Science*, 311, 54
- Xu, Y., Reid, M. J., Menten, K. M., et al. 2009, *ApJ*, 693, 413
- Xu, Y., Moscadelli, L., Reid, M. J., et al. 2011, *ApJ*, 733, 25
- Xu, Y., Li, J. J., Reid, M. J., et al. 2013, *ApJ*, 769, 15
- Xu, Y., Reid, M., Dame, T., et al. 2016, *Science Advances*, 2, e1600878
- Xu, Y., Bian, S. B., Reid, M. J., et al. 2018, *A&A*, 616, L15
- Yao, J. M., Manchester, R. N., & Wang, N. 2017, *ApJ*, 835, 29
- Zhang, B., Zheng, X. W., Reid, M. J., et al. 2009, *ApJ*, 693, 419
- Zhang, B., Reid, M. J., Menten, K. M., & Zheng, X. W. 2012b, *ApJ*, 744, 23
- Zhang, B., Reid, M. J., Menten, K. M., Zheng, X. W., & Brunthaler, A. 2012a, *A&A*, 544, A42
- Zhang, B., Reid, M. J., Menten, K. M., et al. 2013, *ApJ*, 775, 79
- Zhang, B., Moscadelli, L., Sato, M., et al. 2014a, *ApJ*, 781, 89
- Zhang, S., Xu, Y., & Yang, J. 2014b, *AJ*, 147, 46